
Parton distribution functions in the low-energy limit

A DESY Summer Student Report

written by

Pascal Stienemeier

(University of Hamburg, Germany)

supervised by

Markus Diehl



September 7, 2016

Abstract

Looking up the composition of the proton one finds its constituents to be two up quarks and one down quark. For particle collisions however, this picture is not accurate. We instead describe the momentum distribution of the constituents by using *Parton Distribution Functions* (PDFs), derived from elaborate fitting of various experimental data. But do these PDFs still fit to the model of a three constituent proton at low energies?

To find an answer to this question, I compared several commonly used PDFs evolving them to lower energies using the DGLAP equation which was solved via the Mellin moments.

Overall, no PDF set could be found being consistent with the idea of a proton consisting of only valence quarks. One of the sets provided an antiquarkless proton at very low energies but the gluon distribution for this set did not vanish at all and in fact was negative.

Contents

1	Introduction	1
2	Theoretical Background	2
2.1	Parton distribution functions	2
2.2	Evolution of PDFs - The DGLAP equation	4
3	Results	7
3.1	The running coupling constant α_S	7
3.2	Contribution of the low-x region	8
3.3	Influence of higher orders	10
3.4	Uncertainties between different sets	11
3.5	Zeros of Mellin moments	15
4	Conclusion	18

1 Introduction

Today's particle physics experiments are usually very large particle accelerators colliding (anti-)electrons and (anti-)protons in order to challenge the consistency of our current Standard Model of particle physics. If we want to understand the details of what happens in proton-(anti-)proton collisions, it is crucial to have a very good description of the colliding particles, the protons, at hand.

A first attempt was proposed by Richard Feynman in 1969 (Ref. [8]). He suggested what we today call the *QCD parton model*. This model describes the proton to be a composition of point-like constituents, the *partons*. Scatterings on this proton could thus be described as scatterings on one of these partons instead of the proton as a whole. Today we know that these partons are either gluons or quarks inside the proton.

Unfortunately, one encounters infrared singularities in the attempt to describe the whole scattering perturbatively. The QCD Landau pole leads to a dramatically increasing coupling constant rendering the perturbative approach hopeless. The most favoured solution to this problem is given by the *factorisation theorem*. It states that the total computation of the cross section can be split into two parts: The large scale, the partonic cross sections calculable perturbatively independent of the incoming proton and the low scale, the parton distributions only dependent on the incoming proton and independent on the hard scattering process.

Although the parton distribution functions are not dependent on the specific hard scattering process, they are dependent on the characteristic energy of the scattering process corresponding its resolution. Figuratively speaking, a gluon at one energy scale can turn out to be a superposition of two gluon states and a quark states at a higher scale.

To have predictions for not just a single energy scale, we need a way to conclude the parton distribution functions at any scale. This evolution is provided by the DGLAP equation (Ref. [3], Ref. [6] and Ref. [11]) named after Dokshitzer, Gribov, Lipatov, Altarelli and Parisi, given the PDFs are known at one scale.

Usually, the PDFs are evolved to higher energy scales which is certainly possible thanks to the asymptotic freedom of QCD. In this Report however, we want to pursue another objective. Here, we want to evolve the PDFs to lower energies in order to check for the existence of antiquarks and gluons at low energy scales. Early endeavour based on this idea can be found in Ref.[14], Ref.[9] and Ref.[10].

2 Theoretical Background

This chapter discusses the basic properties of parton distribution functions and their scaling behaviour. It is based on Ref. [1] and Ref. [7].

2.1 Parton distribution functions

To describe deep inelastic scattering processes, it is convenient to consider a large momentum frame of the colliding protons. In this frame, the momenta of the partons are almost collinear with the momentum of the colliding protons. Each parton then carries a momentum fraction x of the protons total longitudinal momentum. The *parton distribution functions* (PDFs) represent the probability densities to find a specific parton with a momentum fraction x of the proton.

Such a PDF for the valence up quarks is shown in Fig.1(a) for an energy scale of $Q = 1.3$ GeV. The contribution of the valence quarks is determined by the difference between up quarks and anti up quarks. This is justified by the assumption that due to quarks being produced in pairs there are as much up-type sea quarks as there are antiup-type sea quarks.

As the proton is supposed to have a total number of 2 valence up quarks, we find the integral of the distribution shown in Fig.1(a) to be

$$\int_0^1 (u(x) - \bar{u}(x)) dx = 2 \quad (2.1)$$

This equality holds for every energy scale and is referred to as the *number sum rule* because it represents up quark number in the proton.

A similar rule accounts for the distribution of the down quarks shown in Fig.1(b). The corresponding number sum rule for the down quarks is given by

$$\int_0^1 (d(x) - \bar{d}(x)) dx = 1 \quad (2.2)$$

Besides considering the numbers of quarks in the proton, it is also interesting to have a look at the momentum fractions the partons in the proton carry. This momentum

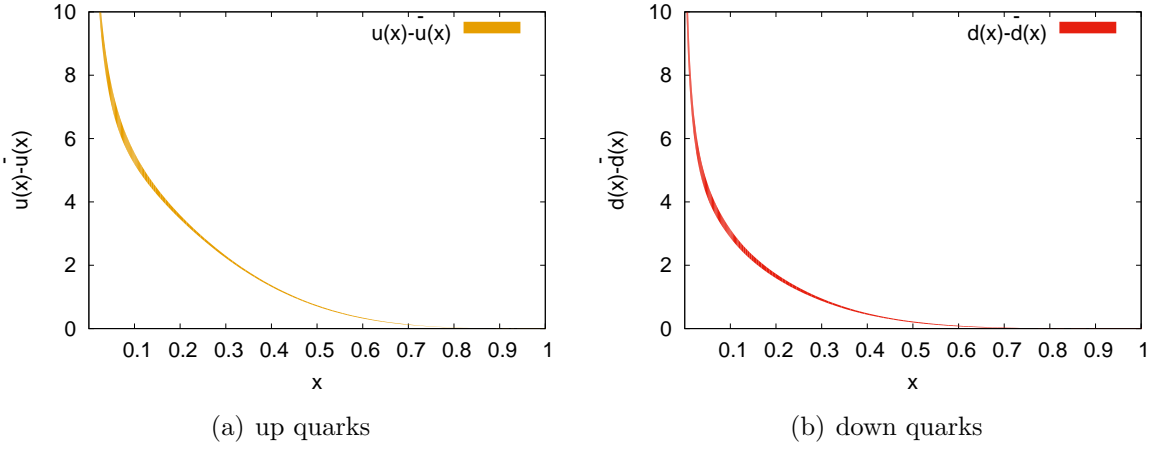


Fig. 1: Typical distributions of up quarks and down quarks in the proton.

distribution is shown for all the quarks in Fig.2(a) using the definition

$$\Sigma(x) := \sum_q q(x) + \bar{q}(x) \quad (2.3)$$

Neglecting the presence of sea quarks in the proton and assuming an even distribution of the protons momentum among the three valence quarks, we would expect the momentum distribution of quarks to show a maximum at $x \approx \frac{1}{3}$. The contribution of sea quarks and gluons however shifts this peak to $x \approx 0.1$.

Integrating these distributions we can determine the total momentum fractions carried by quarks and gluons. For the two distributions shown in Fig.2(a) and Fig.2(b) we find $\int_0^1 x \Sigma(x) dx \approx 0.61$ and $\int_0^1 x g(x) dx \approx 0.39$. From this we can infer that the quarks themselves only carry slightly more than half of the protons total momentum whereas the rest is carried by the gluons.

Due to momentum conservation, we find another connection between the quark distribution and the gluon distribution to be valid at every energy scale - the *momentum sum rule*

$$\int_0^1 x (\Sigma(x) + g(x)) dx = 1 \quad (2.4)$$

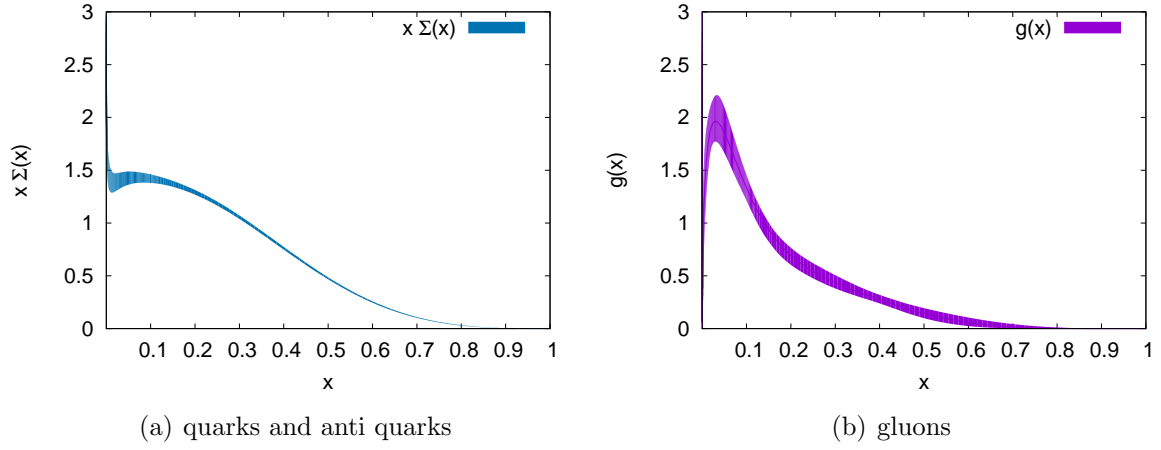


Fig. 2: Typical momentum distributions of partons in the proton.

2.2 Evolution of PDFs - The DGLAP equation

The resolution of a collision is proportional to the momentum transfer q so that a more detailed level of structure is revealed at higher energies. For this reason, the previously discussed parton distributions are just like the coupling constant α_S dependent on the energy scale μ . Their scale dependence is described by the DGLAP equations (Ref. [7]):

$$\begin{aligned} \frac{\partial}{\partial \ln(\mu^2)} \Delta(x, \mu^2) &= \frac{\alpha_S(\mu^2)}{2\pi} P_{qq}^{NS}(x, \mu^2) \otimes \Delta(x, \mu^2) \\ \frac{\partial}{\partial \ln(\mu^2)} \begin{pmatrix} \Sigma(x, \mu^2) \\ g(x, \mu^2) \end{pmatrix} &= \frac{\alpha_S(\mu^2)}{2\pi} \begin{pmatrix} P_{qq}^S(x, \mu^2) & 2n_f P_{qg}(x, \mu^2) \\ P_{gq}(x, \mu^2) & P_{gg}(x, \mu^2) \end{pmatrix} \otimes \begin{pmatrix} \Sigma(x, \mu^2) \\ g(x, \mu^2) \end{pmatrix} \end{aligned} \quad (2.5)$$

Where n_f is the number of light quark flavours, by \otimes we denote the Mellin convolution

$$[P \otimes q](x) := \int_x^1 P\left(\frac{x}{\xi}\right) \cdot q(\xi) \frac{d\xi}{\xi} \quad (2.6)$$

and P_{qq}^{NS} , P_{qq}^S , P_{qg} , P_{gq} and P_{gg} are evolution kernels called *splitting functions* that can be expanded in powers of the coupling constant α . Figuratively speaking, the splitting function P_{xy} corresponds to the probability for a particle y to emit a particle x . Two of these splitting functions are shown in Fig.3. Fig.3(a) shows the splitting function P_{qq} at leading order. Whereas splittings from quarks to antiquarks are not possible at leading order, higher orders also allow processes like this shown in Fig.3(b).

There are two different DGLAP equations to be solved. Whereas the evolution of the *flavour singlet* $\Sigma(x) := \sum_q (q(x) + \bar{q}(x))$ is coupled to the evolution of the gluon distri-

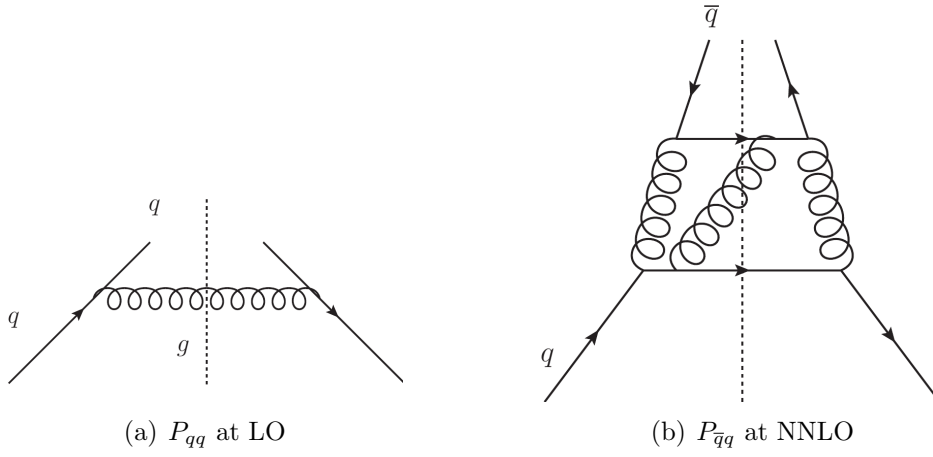


Fig. 3: Two Feynman graphs corresponding to splitting functions.

bution $g(x)$, the *flavour non-singlet* $\Delta(x) := \sum_q (q(x) - \bar{q}(x))$ evolves separately.

A common way to solve the DGLAP equation is to Mellin transform the parton distributions and write the DGLAP equation in terms of the Mellin moments according to

$$\gamma_{qq}(j, \mu^2) := \int_0^1 x^{j-1} P_{qq}(x, \mu^2) dx \quad q(j, \mu^2) := \int_0^1 x^{j-1} q(x, \mu^2) dx \quad (2.7)$$

The Mellin transforms of the splitting functions are called *anomalous dimensions*. Due to the convolution theorem for the Mellin convolution, this simplifies the convolution in the DGLAP equation to become a multiplication

$$\begin{aligned} \frac{\partial}{\partial \ln(\mu^2)} \Delta(j, \mu^2) &= \frac{\alpha_S(\mu^2)}{2\pi} \gamma_{qq}^{NS}(j, \mu^2) \cdot \Delta(j, \mu^2) \\ \frac{\partial}{\partial \ln(\mu^2)} \begin{pmatrix} \Sigma(j, \mu^2) \\ g(j, \mu^2) \end{pmatrix} &= \frac{\alpha_S(\mu^2)}{2\pi} \begin{pmatrix} \gamma_{qq}^S(j, \mu^2) & 2n_f \gamma_{qg}(j, \mu^2) \\ \gamma_{gq}(j, \mu^2) & \gamma_{gg}(j, \mu^2) \end{pmatrix} \cdot \begin{pmatrix} \Sigma(j, \mu^2) \\ g(j, \mu^2) \end{pmatrix} \end{aligned} \quad (2.8)$$

Analytical solutions to these equations can be obtained for the non-singlet case and the singlet case for $j = 2$ by rewriting the scale dependence of the DGLAP equation in terms of $\alpha(\mu)$. An explicit calculation of the resulting integral allows to compute the values of the moments $\Delta(j, \mu^2)$, $g(j, \mu^2)$ and $\Sigma(j, \mu^2)$ for specific j and known values of the moments at any energy scale.

To also compute the evolutions for which an analytical solution was not possible, the Runge-Kutta-method (Ref. [2]) was used to solve the integrals in different orders of α_S up to NNLO. The required β -functions were taken from Ref. [4]. For the splitting functions

for LO and NLO we relied on Ref. [7] and Ref. [13] & Ref. [15] were used for the NNLO splitting functions.

A cross check for our calculation was possible using the sum rules we found in Chap.2.1. These sum rules also apply to the anomalous dimensions and lead to the useful relations:

$$\gamma_{qq}(j=2, \mu^2) + \gamma_{gq}(j=2, \mu^2) = 0 \quad 2n_f \gamma_{qg}(j=2, \mu^2) + \gamma_{gg}(j=2, \mu^2) = 0 \quad (2.9)$$

As an additional test, we compared the anomalous dimensions for j=2 with Ref. [12].

3 Results

3.1 The running coupling constant α_S

For the renormalisation of a quantum field theory, it is necessary to redefine the coupling constants that originally appear in the Lagrangian in order to remove UV divergences. During dimensional regularisation, an energy scale parameter μ is introduced in order for the coupling constant to stay dimensionless. This redefinition of the coupling constants leads to them loosing their characteristic constancy - they become scale dependent.

The so called running of the QCD coupling constant is governed by the renormalisation group equation

$$\beta(\alpha) = \mu^2 \frac{\partial \alpha}{\partial \mu^2} \quad (3.1)$$

This equation can be solved by expanding $\beta(\alpha) = -\alpha^2(\beta_0 + \beta_1\alpha + \beta_2\alpha^2 + \dots)$ to compute the scale dependence of the coupling constant α .

Taking values for β up to next-to-next-to-leading order (NNLO) from Ref. [4], we computed the evolution of α from energies of 1.3 GeV to lower energies. As this energy is below the charm mass, it was sufficient for our analysis to consider only 3 light quark flavours. The resulting behaviour of α is shown in Fig. 4 The asymptotic freedom which

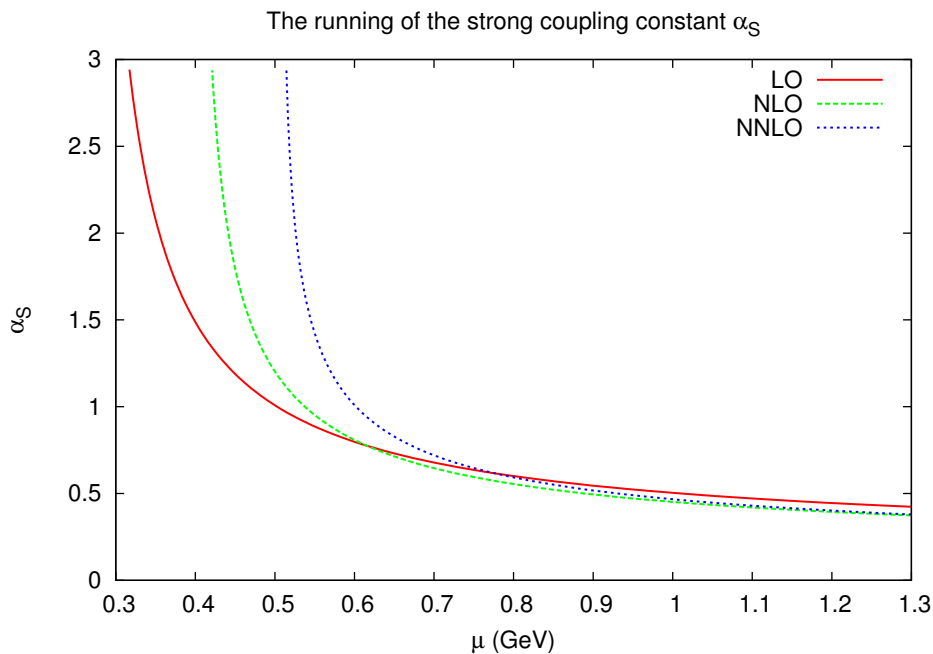


Fig. 4: The running coupling constant $\alpha(\mu)$ for the PDF sets CT14lo, CT14nlo and CT14nnlo.

is characteristic for QCD can be observed clearly in all orders of calculation. Nevertheless, the Landau pole appears at different scales μ . Whereas α exceeds the value of 3 for $\mu = 0.32$ at leading order (LO), the same value is already reached for $\mu = 0.51$ at NNLO because of the higher order contributions.

3.2 Contribution of the low-x region

For all data including plots shown in this report, we used the PDF datasets provided by the LHAPDF6 library (Ref. [5]). It is a commonly used successor to the Fortran PDF library LHAPDF. For the generation of the 15 PDF sets we used and for our calculations, effective parton distributions were used taking only 3 light quark flavours u , d , s into account. It is convenient to use this low-energy approximation of QCD because more massive quark flavours would have a negligible effect on the low-energy results.

In order to interpret the following results properly, we first take a look at the reliability of the PDF sets we used in the low-x region. As measurements in this region are very difficult to perform and therefore not yet available, the reliability of the PDFs greatly decreases approaching low-x values in addition to their increasing uncertainties.

To obtain initial values for the PDF evolution of the Mellin moments, we integrated the available PDF datasets at $\mu = 1.3$ GeV. To estimate the effect of additional uncertainties in the low x region on our evolution, we divided the integration into three sectors. The first sector includes x values lower than 0.0001, the second sector includes values ranging from 0.0001 to 0.1 and the last one includes the rest from 0.1 to 1.

The contributions from the lower x values to the total integral are shown in Fig.5 for the moment $g(j = 1.5) = \int_0^1 \sqrt{x} g(x) dx$ for the variety of sets we considered. Fig.5(a) shows two important aspects. On the one hand, negative contributions are observable for some sets. The moments are not forced to stay positive in every set in order to get a better fit to experimental data. At least at this point, the interpretation of the PDFs as possibility distributions is no longer valid.

On the other hand, the contribution's absolute values are highest for this moment. Although this was expected because the gluon distribution in particular raises for low x, it means that especially low-j gluon moments are supposed to have a higher additional uncertainty originating from missing experimental data in the low-x region.

Higher Mellin moments of the gluon distribution as shown in Fig.6 are less influenced

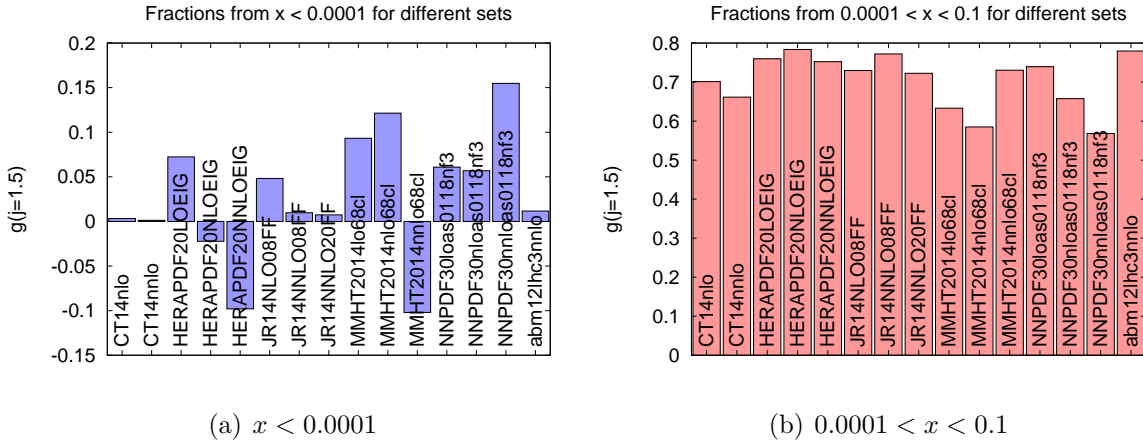


Fig. 5: Fractions from low x values contributing to $\int_0^1 \sqrt{x} g(x) dx$.

by contributions from very low x regions. The maximum contribution to be found here carries less than $10^{-4}\%$ of the total integral. For this Mellin moment however, the relative contribution of the middle ranged x values between 0.0001 and 0.1 shows the largest relative variance ranging from 10% up to 30%. This again states the fact that the gluon distribution is dominated by low x contributions even if these are suppressed by weighting them with x^2 .

As discussing every contribution for every set in detail would leave the scope of this

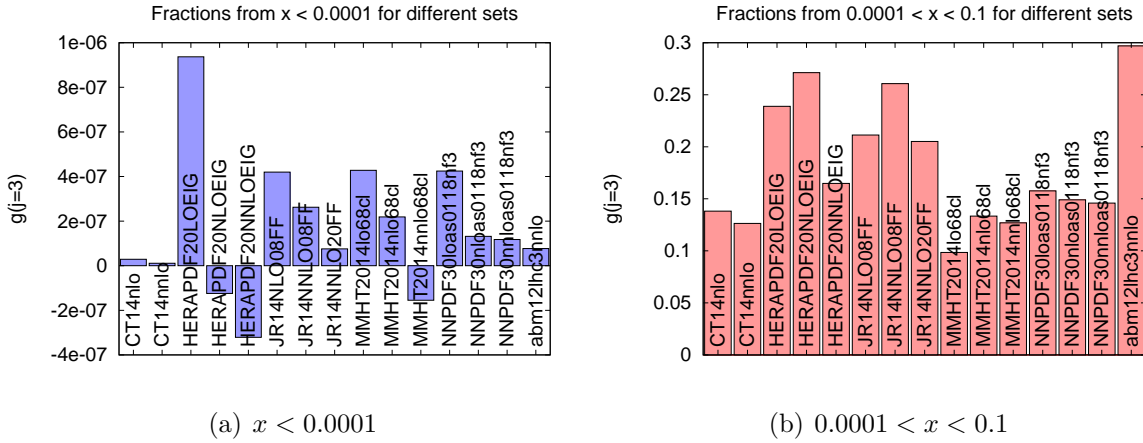


Fig. 6: Fractions from low x values contributing to $\int_0^1 x^2 g(x) dx$.

report, the range of the contributions from low x values for all gluon moments is summarized in Tab.1.

The fractions of low x values to the Mellin moments of other PDFs are overall smaller and much more uniformly distributed.

x	$j = 1.5$	$j = 2$	$j = 2.5$	$j = 3$
0.0001...0.1	0.6...0.8	0.4...0.6	0.2...0.4	0.1...0.3
10^{-9} ...0.0001	-0.1...0.15	-0.001...0.002	$-2 \cdot 10^{-5}$... $5 \cdot 10^{-5}$	$-3 \cdot 10^{-4}$... 10^{-6}

Tab. 1: Contributions of the low-x fractions to the gluon moments.

3.3 Influence of higher orders

An important factor for the evolution of the PDFs is the order of α_S taken into account for the computation. This applies to the creation of the PDF sets influencing the initial values of the evolution at small α on the one hand and the evolution itself on the other hand.

To the present day, splitting functions necessary to compute PDFs and their evolution were computed up to $\mathcal{O}(\alpha^2)$ (Ref. [15], Ref. [13]). As higher orders are not available explicitly, the only way to estimate the stability of the computations regarding higher orders is to compare the changes between lower orders.

Such a comparison is shown by Fig.7 for the gluon evolution. For the evolution of the gluon's momentum distribution shown in Fig.7(a), the difference between NLO and NNLO is much smaller than the difference to the leading order. In fact, the discrepancy between NLO and NNLO is completely neglectible compared to the uncertainties of the PDF sets.

Similar effects can be seen for higher moments of the gluon distribution in Fig.7(b). Although there is a larger difference between the initial values for NLO and NNLO, evolving them to larger values of α leads to both orders being in agreement within their uncertainties.

Overall we can therefore expect that the moments of the gluon distributions are steady considering higher orders of α .

Another behaviour however can be seen in Fig.8 for the evolution of the antiquark distribution. Although the antiquark distribution contributes to both $\Delta(j, \mu^2)$ and $\Sigma(j, \mu^2)$ which evolve separately, it can be reobtained at every point of the evolution via $\bar{q}(j, \mu^2) = \frac{1}{2} (\Sigma(j, \mu^2) - \Delta(j, \mu^2))$.

For the evolution of the corresponding momentum distribution given by the HERA-PDF20 set, we see that the NNLO computation leads to a major deviation from NLO which is even larger for high values of α .

For higher moments of \bar{q} , even stranger behaviour shows up. Although LO and NNLO

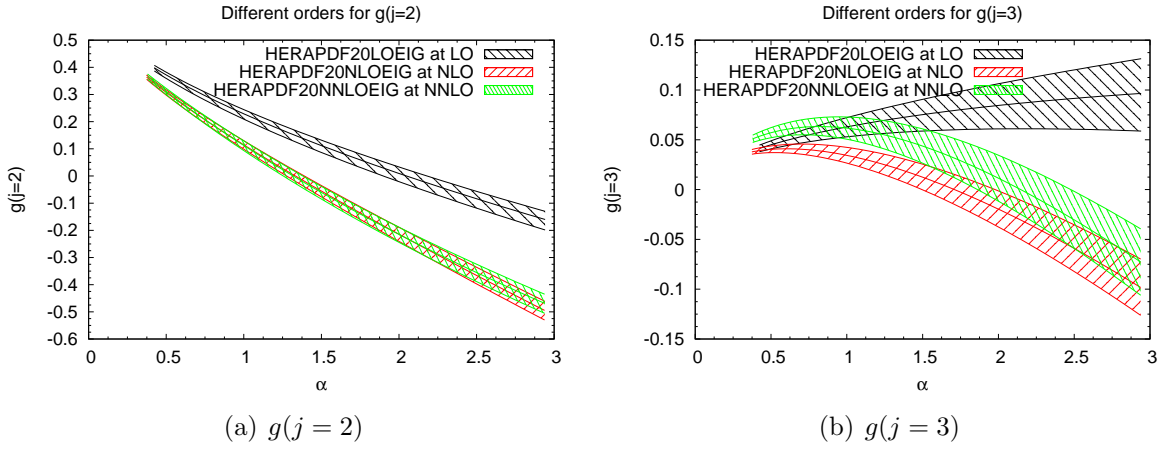


Fig. 7: Comparison of different orders for the gluon evolution.

are in agreement here, the NLO computation deviates. For these reasons, the NNLO computations of the \bar{q} moments at high values of α in this set have to be interpreted with caution.

In all other sets considered for which three different orders were available, the NLO and the NNLO computations for the antiquark moments are in better agreement. The same accounts for the moments of the quark distributions. Thus, in most cases the NNLO is supposed to be sufficiently reliable.

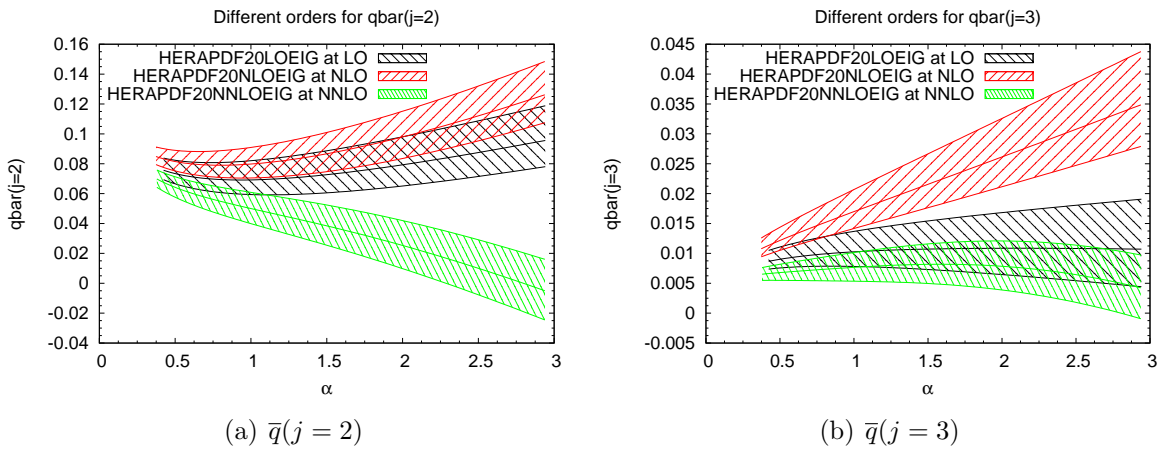


Fig. 8: Comparison of different orders for the antiquark evolution.

3.4 Uncertainties between different sets

Another important factor contributing to additional uncertainties are the different approaches used by different collaborations to fit the experimental data in order to create

the PDF sets in the first place. As there is not one single approach superior to all the others, a comparison of the various available PDF sets is necessary to estimate the uncertainty due to the choosing of the set.

To compare the effects using different sets, two Mellin moments will be discussed explicitly. At first, such a comparison is shown in Fig.9 for the moment $g(j=3)$.

At LO three sets were compared. Although they are similar for large μ , a difference shows up at lower energies approaching the QCD Landau pole. The fact that some sets evolve to lower μ values than others originates back to different values for $\alpha(\mu = 1.3 \text{ GeV})$ used in the sets. As we stop the PDF evolution when α exceeds a value of 3, those sets with lower initial values for α evolve to lower values for μ .

At LO there are some sets such as HERAPDF that do not diverge even for low μ values whereas others show the effects of the Landau pole earlier. At NLO the behaviour of different PDF sets approaching the Landau pole is even more diverse. Some sets drop to negative values and at the same time others show larger values. So especially the behaviour of the sets at low μ values is much more unknown than displayed by just the own uncertainties of the PDF sets.

Taking into account the NNLO contribution, all sets tend to lower values for low μ and most of them cross the zero, so the NNLO contribution is an important factor when it comes to the determination of zeros.

The Mellin moment $\bar{q}(j = 2)$ shown in Fig.10 exhibit slightly less dependence on the PDF set. At LO and NLO the momentum distributions of the antiquarks are in agreement with each other for a large range of energy scales compared to their intrinsic uncertainties. In addition to that they show an extensive constancy for $\mu > 0.6 \text{ GeV}$ which is not to be expected trivially.

The NNLO contribution to this moment changes its behavior more drastically. In all sets, the antiquark moment approaches zero only after taking the NNLO into account. The corresponding plots for the moments that could not be presented here show uncertainties due to the chosen set similar to the $\bar{q}(j = 2)$ moment. Some of these were not shown here because of very large uncertainties of the low- j gluon moments. These large uncertainties appear for some sets which force the PDFs to stay positive at points where the moments as predicted by other sets approach negative values.

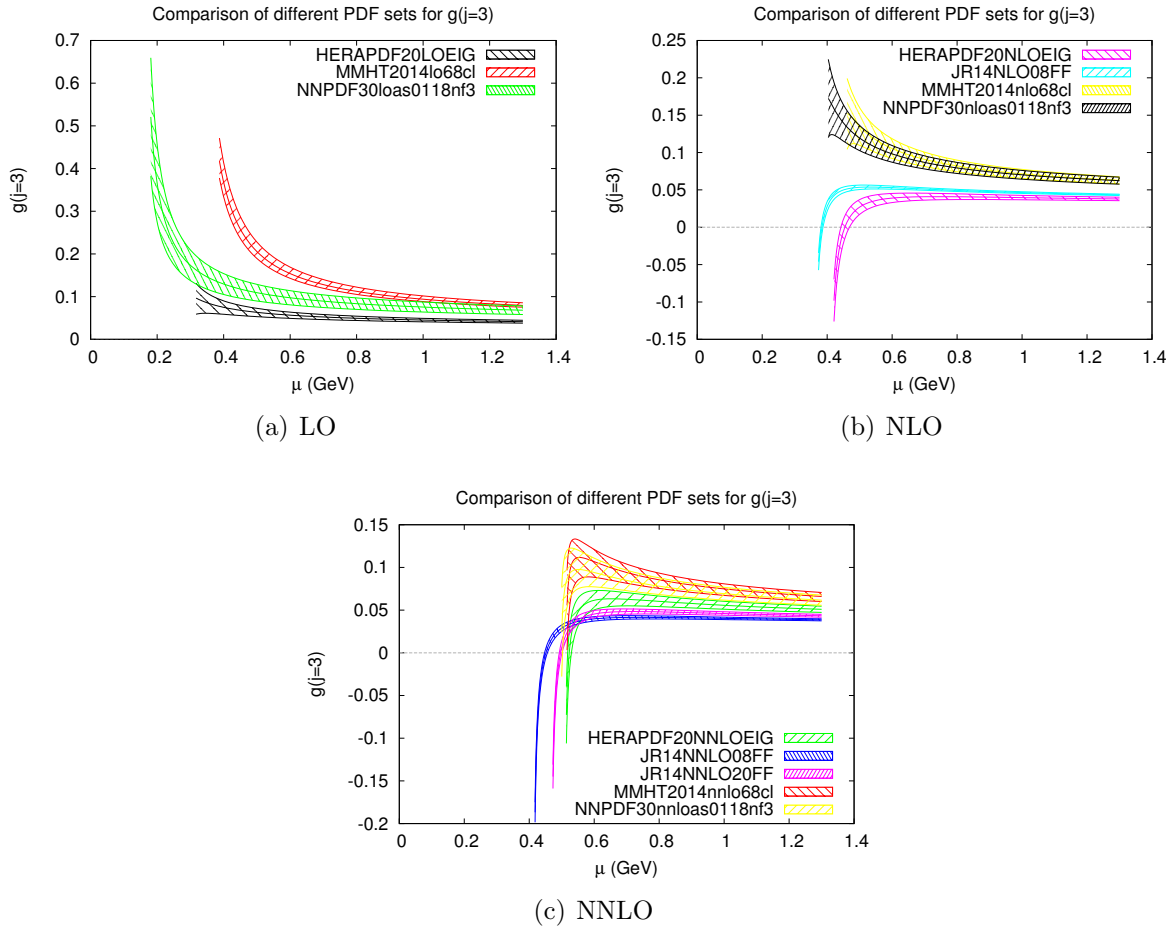


Fig. 9: Comparison of different sets for $g(j = 3)$ at three different orders. At NLO and NNLO the set CT14nlo is not displayed to guarantee clarity of the plots. Its data behaves similar to the MMHT set. In addition to that at NNLO the set abm12lhc3 is not displayed because its data is similar to JR14NNLO08.

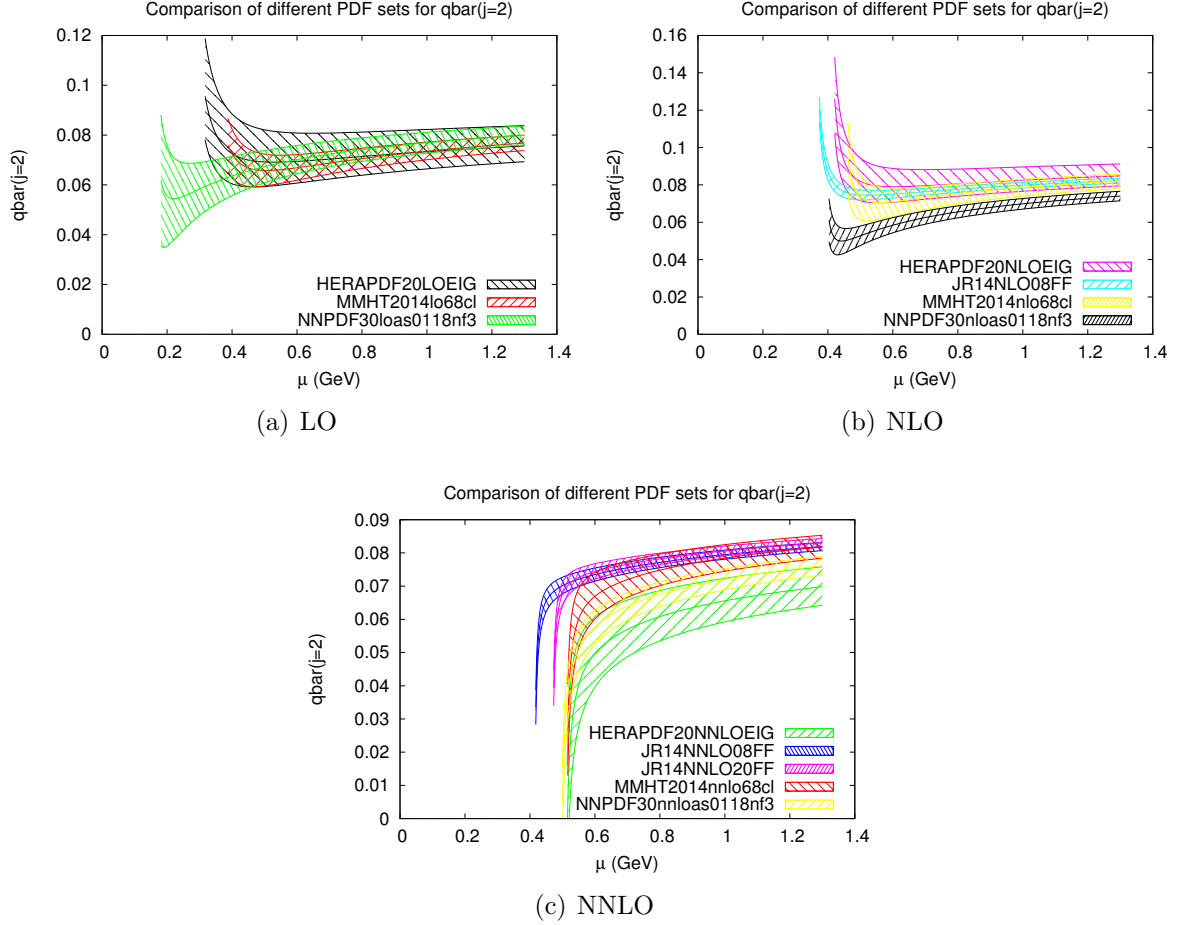


Fig. 10: Comparison of different sets for $\bar{q}(j=3)$ at three different orders. At NLO and NNLO the set CT14nlo is not displayed to guarantee clarity of the plots. Its data lies between the NNPDF30 set and the JR14 sets. In addition to that at NNLO the set abm12lhc3 is not displayed because its data is similar to JR14NNLO08.

3.5 Zeros of Mellin moments

The main question this report is devoted to, is to check the existence of gluons and anti-quarks in the proton at low energies. As the gluon distribution itself diverges approaching low x values and is therefore not integrable, we consider higher Mellin moments of the gluon and antiquark distributions. If all moments would show zeros at the same energy scale, this would be a strong indication of the distributions themselves to vanish at this energy corresponding to a gluonless and antiquarkless proton.

We checked this criteria for the gluon moments $g(j)$ and the antiquark moments $\bar{q}(j)$ for $j \in \{1.5, 2, 2.5, 3\}$ and considered 15 different PDF sets.

Unfortunately, only one of the sets we considered, namely abm12lhc3nnlo was rather consistent with the idea of a gluonless proton. The corresponding plots are displayed in Fig.11(a). If plotted against μ , all moments for $j \leq 2$ seem to coincide at energies slightly larger than 0.4 GeV. Due to the QCD Landau pole compressing large variations in α into small variations in μ , it is hard to judge a common zero of all moments just from Fig.11(a). To overcome this issue, the same moments are plotted against α in Fig.11(b). Due to the asymptotic freedom, α decreases for higher μ and therefore the intersections of the moments can be found at the right side of the plot.

Plotting the moments against α , the deviation of $g(j = 1.5)$ is more obvious. At $\mu = 1.4$ where all other moments are equal to zero, the moment $g(j = 2)$ is about 3σ below zero so even the most auspicious set does not provide a gluonless proton at any scale.

The second best set for which all gluon moments might disappear is shown in Fig.12.

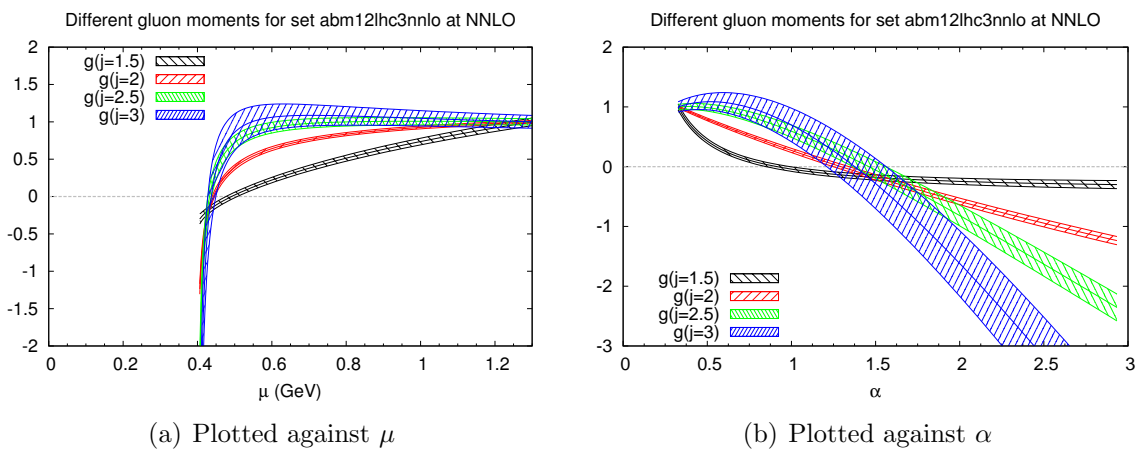


Fig. 11: The set for which the zeros of all gluon moments coincide best. All moments in these plots are normalized to an initial value of 1.

Although it is possible for all gluon moments to be zero at the same time according to the uncertainties, this holds mainly for the reason that the uncertainties are comparably large. The mean of the lowest displayed gluon moment $g(j=2)$ does not even cross zero at all. Again, if plotted against α for a better resolution, the zeros of the gluon moments clearly do not match.

Overall none of 15 sets includes the possibility for all gluon moments to vanish at a certain energy scale. Moreover, most of the sets clearly exclude this possibility.

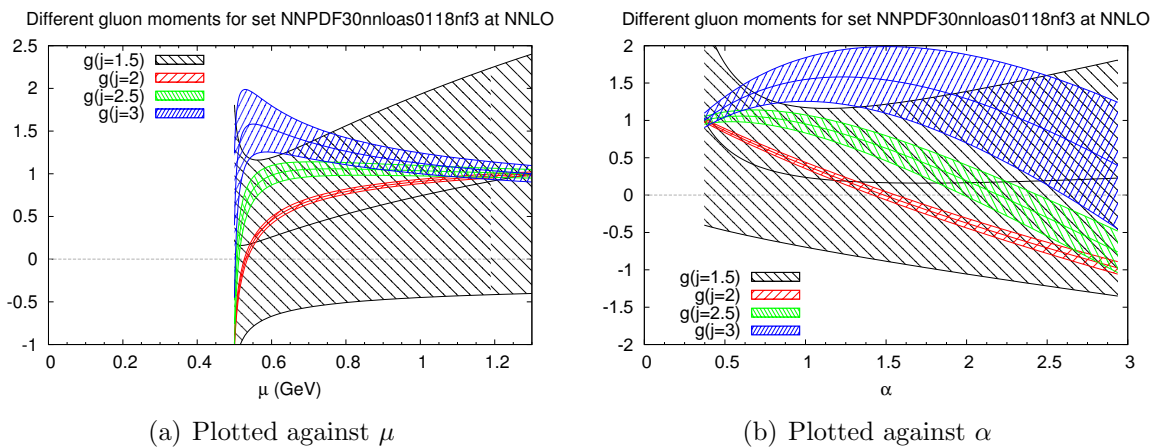


Fig. 12: Another set for which the zeros of all gluon moments are close to each other. All moments in these plots are normalized to an initial value of 1.

Considering the antiquark distribution, common zeros of its moments are even less often to find. No dataset up to NLO shows common zeros of all \bar{q} moments. For more than half of these sets the moments of \bar{q} stay positive for all values of μ . An example of this is given by Fig.13.

At NNLO, there is one case in which coinciding zeros of all moments are possible. This most promising plot be seen in Fig.14. For more clarity it is plotted against μ in Fig.14(a) and against α in Fig.14(b).

Although the antiquark moments clearly overlap for $\alpha \approx 2.8$, interpreting the next-to-next-to leading order of a perturbative approach at this point is risky so that this result may not be taken for granted.

If the gluon moments for this set would also be zero at the same energy, this set would provide a proton consisting of only valence quarks. These gluon moments are shown in Fig.15. Unfortunately, the zeros of the gluon moments clearly do not overlap. Moreover,

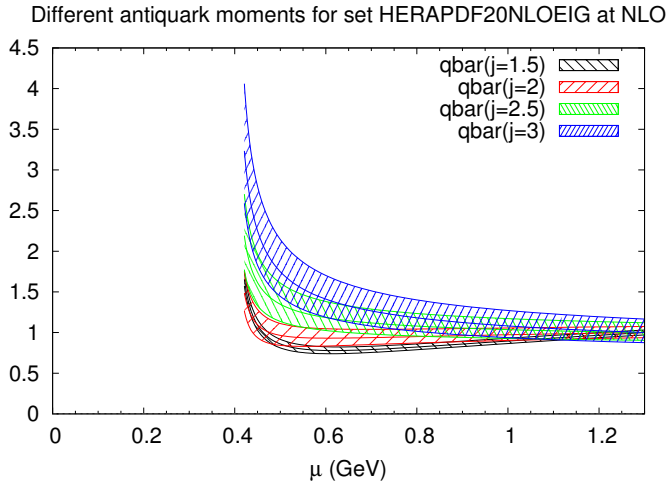


Fig. 13: The \bar{q} moments often do not show zeros at all. All moments in this plot are normalized to an initial value of 1.

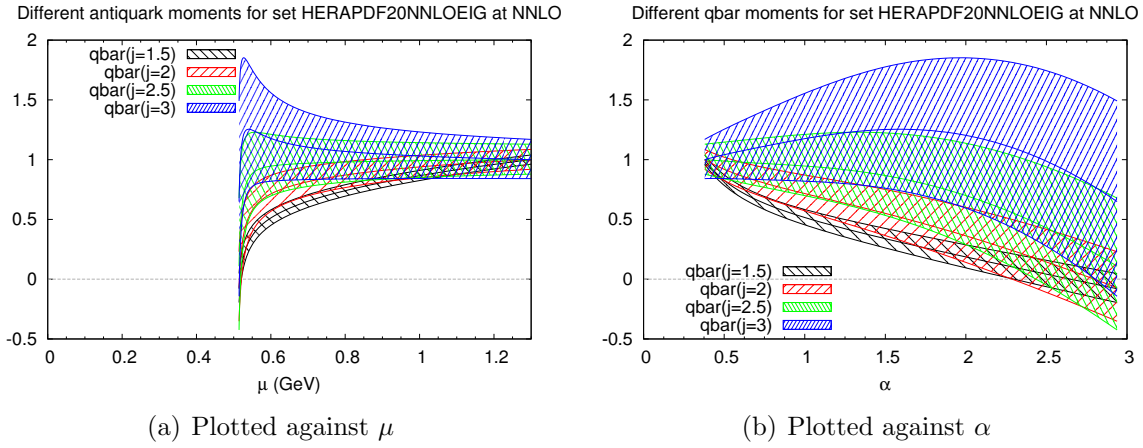


Fig. 14: For the displayed set a coinciding zero for all the \bar{q} moments is most likely. All moments in these plots are normalized to an initial value of 1.

the gluon moments at this point are without exception negative. The resulting negative gluon distribution at this point stresses the fact that the distributions can no longer be interpreted as probability distributions.

Overall, none of the 15 considered datasets is in agreement with a gluonless and at the same time antiquarkless proton.

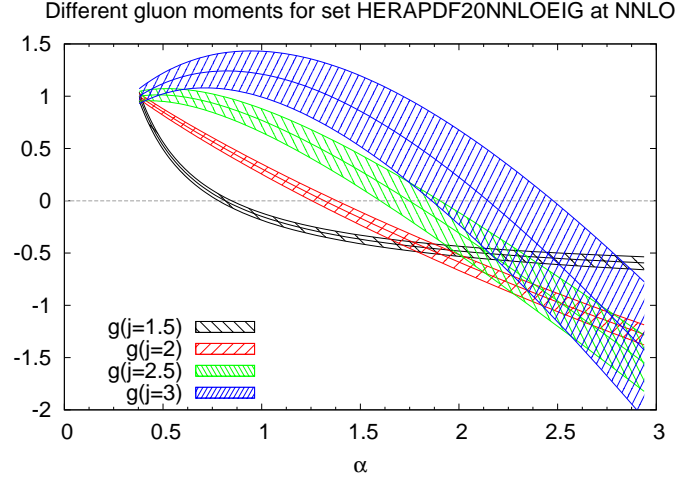


Fig. 15: The gluon moments for the set HERAPDF20NNLOEIG. The antiquark moments of this set are shown in Fig.14(b). All moments in this plot are normalized to an initial value of 1.

4 Conclusion

At the beginning of this report was the question of whether today's parton distribution functions still fit to the model of a proton at rest consisting of only three valence quarks. To find an answer to this question, different commonly used PDF sets were evolved to lower energies using a solution of the DGLAP equations via Mellin moments.

If the proton consisted of only valence quarks, the gluon distribution and the antiquark distribution would decrease to zero approaching lower energies. In this case, their Mellin moments should all vanish at this energy scale.

For the PDF sets considered in this report, none out of 15 datasets showed the possibility for all gluon moments to diminish to zero at the same energy scale and only 1 out of 15 sets agrees with the assumption of all antiquark moments to cross zero at the same energy which in this case corresponds to values of α_S larger than 2.

Combining both results, no PDF set agrees with the model of a gluonless and antiquarkless proton at low energy scales and just one set includes the possibility of antiquarks to be absent at an energy scale for which the gluon distribution is already negative.

References

1. Sept. 1, 2016, http://www.scholarpedia.org/article/QCD_evolution_equations_for_parton_densities.
2. Sept. 4, 2016, https://en.wikipedia.org/wiki/Runge-Kutta_methods.
3. G. Altarelli, G. Parisi, *Nucl. Phys.* **B126**, 298–318 (1977).
4. P. A. Baikov, K. G. Chetyrkin, J. H. Kühn, *Five-Loop Running of the QCD coupling constant*, 2016, eprint: [arXiv:1606.08659](https://arxiv.org/abs/1606.08659).
5. A. Buckley *et al.*, *Eur. Phys. J.* **C75**, 132 (2015).
6. Y. L. Dokshitzer, *Sov. Phys. JETP* **46**, [Zh. Eksp. Teor. Fiz.73,1216(1977)], 641–653 (1977).
7. R. K. Ellis, W. J. Stirling, B. R. Webber, *Camb. Monogr. Part. Phys. Nucl. Phys. Cosmol.* **8**, 1–435 (1996).
8. R. P. Feynman, in *Special Relativity and Quantum Theory: A Collection of Papers on the Poincaré Group*, ed. by M. E. Noz, Y. S. Kim (Springer Netherlands, Dordrecht, 1988), pp. 289–304, ISBN: 978-94-009-3051-3, DOI: [10.1007/978-94-009-3051-3_25](https://doi.org/10.1007/978-94-009-3051-3_25), http://dx.doi.org/10.1007/978-94-009-3051-3_25.
9. M. Gluck, E. Reya, *Nucl. Phys.* **B130**, 76–92 (1977).
10. M. Gluck, R. M. Godbole, E. Reya, *Z. Phys.* **C41**, 667 (1989).
11. V. N. Gribov, L. N. Lipatov, *Sov. J. Nucl. Phys.* **15**, [Yad. Fiz.15,781(1972)], 438–450 (1972).
12. S. A. Larin, P. Nogueira, T. van Ritbergen, J. A. M. Vermaseren, *Nucl. Phys.* **B492**, 338–378 (1997).
13. S. Moch, J. A. M. Vermaseren, A. Vogt, *Nucl. Phys.* **B688**, 101–134 (2004).
14. G. Parisi, R. Petronzio, *Phys. Lett.* **B62**, 331–334 (1976).
15. A. Vogt, S. Moch, J. A. M. Vermaseren, *Nucl. Phys.* **B691**, 129–181 (2004).